Observation of Topologically Protected Edge States in a Photonic Two-Dimensional Quantum Walk

Chao Chen,[1,2] Xing Ding,[1,2] Jian Qin,[1,2] Yu He,[1,2] Yi-Han Luo,[1,2] Ming-Cheng Chen,[1,2] Chang Liu,[1,2] Xi-Lin Wang,[3] Wei-Jun Zhang,[3] Hao Li,[3] Li-Xing You,[3] Zhen Wang,[3] Da-Wei Wang,[4,*] Barry C. Sanders,[1,2,5,6] Chao-Yang Lu,[1,2,†] and Jian-Wei Pan[1,2,‡]

[1]*Hefei National Laboratory for Physical Sciences at the Microscale and Department of Modern Physics, University of Science and Technology of China, Shanghai Branch, Shanghai 201315, China*

[2]*CAS-Alibaba Quantum Computing Laboratory, CAS Centre for Excellence in Quantum Information and Quantum Physics, Shanghai 201315, China*

[3]*State Key Laboratory of Functional Materials for Informatics, Shanghai Institute of Microsystem and Information Technology (SIMIT)*

[4]*Department of Physics, Zhejiang University, Hangzhou, Zhejiang 310027, China*

[5]*Institute for Quantum Science and Technology, University of Calgary, Alberta T2N 1N4, Canada*

[6]*Program in Quantum Information Science, Canadian Institute for Advanced Research, Toronto, Ontario M5G 1Z8, Canada*

(Received 29 May 2018; published 6 September 2018)

Periodically driven systems have displayed a variety of fascinating phenomena without analogies in static systems, which enrich the classification of quantum phases of matter and stimulate a wide range of research interests. Here, we employ discrete-time quantum walks to investigate a nontrivial topological effect unique to a two-dimensional periodically driven system: chiral edge states can exist at the interface of Floquet insulators whose Chern numbers vanish. Thanks to a resource-saving and flexible fiber-loop architecture, we realize inhomogeneous two-dimensional quantum walks up to 25 steps, over an effective 51×51 lattice with tunable local parameters. Spin-polarized chiral edge states are observed at the boundary of two distinct quantum walk domains. Our results contribute to establishing a well-controlled platform for exploring nontrivial topological phases.

DOI: 10.1103/PhysRevLett.121.100502

Beyond fundamental research interests, potential applications to spintronics [1] and topological quantum computation [2] spur extensive investigation into topological phases of well controlled systems. In the past decade, topologically protected edge states have also been shown to exist in periodically driven systems called Floquet topological insulators [3,4]. According to Floquet band theory, a periodically driven system can be treated effectively as being static: its topological phase is classified by a time-independent effective Hamiltonian [5]. Interestingly, some novel topological phenomena without counterparts in static systems, such as anomalous Floquet-Anderson insulators [6–9] and time crystals [10–12], illuminate new topological physics in periodically driven systems where continuous time translational symmetry is broken.

A discrete-time quantum walk (DTQW) describes coherent propagation of a spin-1/2 particle on a lattice, evolving under repeated implementation of a unitary step operator [13–17]. With modified walk protocols, DTQWs can simulate various topological phases classified by symmetries and dimensions [18]. Experimental investigations of the topological properties of one-dimensional DTQWs have been demonstrated in physical systems with photons [19–23] and superconducting circuits [24].

Here, we experimentally investigate topological phenomena of a two-dimensional DTQW (2DQW) in a time-multiplexed architecture [14–16,21]. In our 2DQW model, the Chern number, which indicates chiral edge modes at the boundary of a quantum Hall effect device [25,26], turns out to vanish over the entire parameter space, although topologically protected edge states have been predicted to exist at the boundaries of two different 2DQW domains [27]. Instead, the Rudner winding number [6] characterizes the topological phases of the 2DQW [28,29], which are not incorporated in the periodic table of topological classes for static systems [30]. We confirm the presence of edge states by observing spin-momentum locked edge states with topological robustness at the boundary of a photonic inhomogeneous 2DQW.

Given a single spin-1/2 particle walking on a two-dimensional (2D) periodic lattice, the basis vector is $|x, y, s\rangle$, where s is the internal spin state, and x, y are the coordinates of the walker in the 2D lattice. The unitary operator of a single step is

$$U = T_y R(\theta_2) T_x R(\theta_1), \qquad R(\theta) = e^{-i\sigma_y \theta/2}, \tag{1}$$

where $R(\theta)$ is a spin rotation around the y axis, and T denotes a spin-dependent translation in position space. In the x direction, the translation operator is

$$T_x = \sum_x [|x+1\rangle\langle x| \otimes |\uparrow\rangle\langle\uparrow| + |x-1\rangle\langle x| \otimes |\downarrow\rangle\langle\downarrow|], \quad (2)$$

and likewise for T_y.

According to Floquet band theory, the effective quantum-walk Hamiltonian is obtained from the single-step unitary operator by the equation

$$U(\theta_1, \theta_2) = e^{-iH(\theta_1,\theta_2)t/\hbar}, \quad (3)$$

where t is the time duration of one unitary operation (here we set $t/\hbar \equiv 1$). In quasimomentum space, we obtain the spin-orbit coupling Hamiltonian

$$H(\theta_1, \theta_2) = \int d^2\boldsymbol{k}[E(\boldsymbol{k})\boldsymbol{n}(\boldsymbol{k}) \cdot \boldsymbol{\sigma}] \otimes |\boldsymbol{k}\rangle\langle\boldsymbol{k}|, \quad (4)$$

where $\boldsymbol{\sigma} = (\sigma_x, \sigma_y, \sigma_y)$ is the Pauli matrix vector and the unit vector $\boldsymbol{n} = (n_x, n_y, n_z)$ determines the spin eigenstate at each quasienergy $E(\boldsymbol{k})$. Because of the periodic implementation of U, quasienergy acts as an accumulated phase for the eigenstate after each step and has a periodicity of 2π [27].

For arbitrary parameters, the quasienergy spectrum of $H(\theta_1, \theta_2)$ has a two-band structure and the Chern number is always 0, except the gapless phases for which the quasienergy gaps close at both $E = 0$ and $E = \pm\pi$ [Fig. 1(a) and [31]]. Because of the periodicity of quasienergy, $E = \pi$ coincides with $E = -\pi$. Rudner winding numbers are also labeled in the phase diagram to characterize different topological phases by considering the time dependence of U during one driving period [28,29].

In Figs. 1(c)–1(d), band structures of inhomogeneous 2DQWs with the geometry defined in Fig. 1(b) are shown. If Hamiltonians of $x < 0$ and $x \geq 0$ have distinct winding numbers, edge states are present with quasienergies lying in the band gaps of bulk states and close the gaps around $E = 0$ and $E = \pm\pi$. The implied nontrivial topological

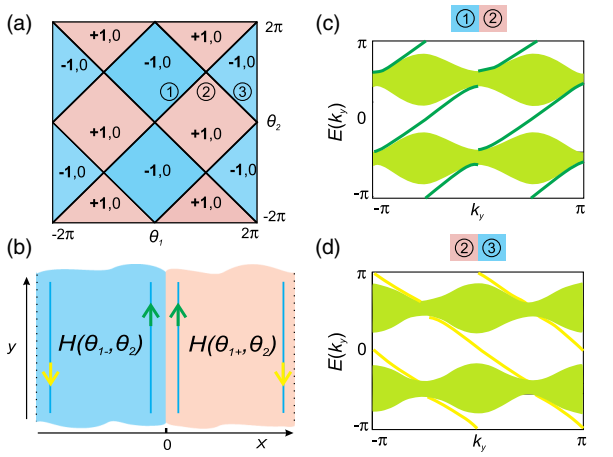

FIG. 1. Phase diagram, inhomogeneous 2DQW, and quasienergy bands. (a) Phase diagram of the 2DQW. Topological phases are distinguished by Rudner winding numbers $W = \pm 1$ (bold), whereas the Chern number is always 0 (normal typeface). Black bold lines indicate the gapless phases, separating the parameter space into distinct phases (magenta and blue). ①–③ represent different parameter choices for 2DQWs. (b) Schematic figure of spatial inhomogeneous 2DQW with effective Hamiltonians $H(\theta_{1-}, \theta_2)$ for $x < 0$ and $H(\theta_{1+}, \theta_2)$ for $x \geq 0$, where $\theta_{1-} \neq \theta_{1+}$ and $\theta_2 = \pi/2$. A finite geometry and periodic boundary conditions in the x direction are assumed (dashed black line). In the y direction, we employ a geometry of infinite length with translational invariance. When the left ($x < 0$) and right ($x \geq 0$) Hamiltonians are described by different winding numbers, chiral edge modes appear, as marked by the green (yellow) arrowed lines at the middle (outer) edge. (c)–(d), Quasienergy bands of the inhomogeneous 2DQWs with parameter choices shown above. Chiral edge states are colored green (yellow) with positive (negative) dispersion corresponding to upward (downward) edge modes in (b). In our experiment, we simulate inhomogeneous 2DQWs with open boundary conditions, so only edge states localized at the middle edge ($x = 0$) are depicted in the band structures.

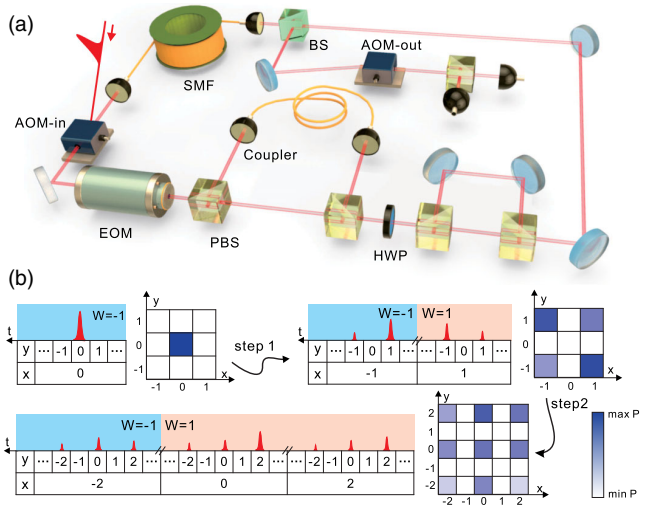

FIG. 2. Experimental implementation of 2DQWs with time-bin encoding. (a) Experimental setup. The initial pulse is generated from an 895 nm pulsed laser with a pulse duration of 15 ps and a repetition frequency of 30 kHz, and is coupled into the circuit by an acousto-optic modulator (AOM). The rotation operations $R(\theta_1)$ and $R(\theta_2)$ are, respectively, implemented by a fast-switching electro-optic modulator (EOM) and a half wave plate (HWP). The two-PBS (polarizing beam splitter) loops are used to realize polarization-dependent optical delays, where the V component is delayed relative to the H component by a 6 m-long single mode fiber (SMF) and 30 cm free-space path difference, representing the translation in the x and y directions, respectively. After every single step, around 3% of photons are reflected by a beam splitter for detection and the transmitted photons continue to propagate through the circuit. (b) Reconstruction of 2D probability distributions. The initial pulse is localized at origin $|0, 0\rangle$. After one 2DQW step, a single pulse is split into four discrete time bins, equivalent to a walker coherently dispersed on a 3×3 lattice with the probabilities of the even sites null. Similarly for the second step and so on.

structure, "quasienergy winding" [5], provides an intuitive understanding of the topological origin in this 2DQW model [31] and some other exotic phenomena unique to periodically driven systems [6].

Being benefited from the fact that quantum interference in quantum walks can be simulated by the wave nature of a coherent light field, we implement inhomogeneous 2DQWs with photons from an attenuated laser pulse [14–16,33]. The internal spin states ($|\uparrow\rangle$, $|\downarrow\rangle$) of a walker are represented by photon polarizations ($|H\rangle$, $|V\rangle$) and the 2D spatial positions are encoded in discrete time bins at two different time scales [16].

As shown in Fig. 2(a), a single-step 2DQW, as defined in Eqs. (1) and (2), is realized by a round trip through the circuit [31]. The efficiency of a round trip is 63% [31]. In Fig. 2(b), we show the mapping between the time-bin sequence and the 2D spatial lattice, and a coordinate (x, y) corresponding to a site on the 2D lattice is used to label each discrete time bin. Because of temporal separation, the fast-switching EOM can implement different $R(\theta_{1\pm})$ on time bins of $x < 0$ and $x \geq 0$ to realize inhomogeneous 2DQWs of distinct topological phases ($W = \pm 1$). The dynamics of a 2DQW can be traced by reconstructing the 2D probability distributions $P(x, y; n)$ from the photon statistics of the output time-bin sequence, where n is the step number. Owing to loss accumulated by 25 round trips, the final state diminishes to the single-photon level before being coupled out of the circuit and detected by superconducting nanowire single-photon detectors [31]. All experimental results of $P(x, y; n)$ are averaged over more than 10^4 detected incidents.

First, we choose Hamiltonians $H(\theta_{1\pm}, \theta_2)$ belonging to different topological phases $W = \pm 1$ and $W = \mp 1$ corresponding to the cases of Figs. 1(c) and 1(d), respectively. As shown in Fig. 3(a) [3(b)], edge states propagating upward (downward) from the origin are observed near the boundary at $x = 0$ with initial polarization $|H\rangle$ ($|V\rangle$), where the initial polarization is selected to have a large overlap with the edge modes. In contrast to the localized edge modes at $x = 0$, the bulk-mode component spreads ballistically into the bulk. During evolution, edge-state wave packets display almost no expansion, manifesting linear dispersion around $E = 0$ and $E = \pm\pi$ shown in Figs. 1(c) and 1(d). To compare the

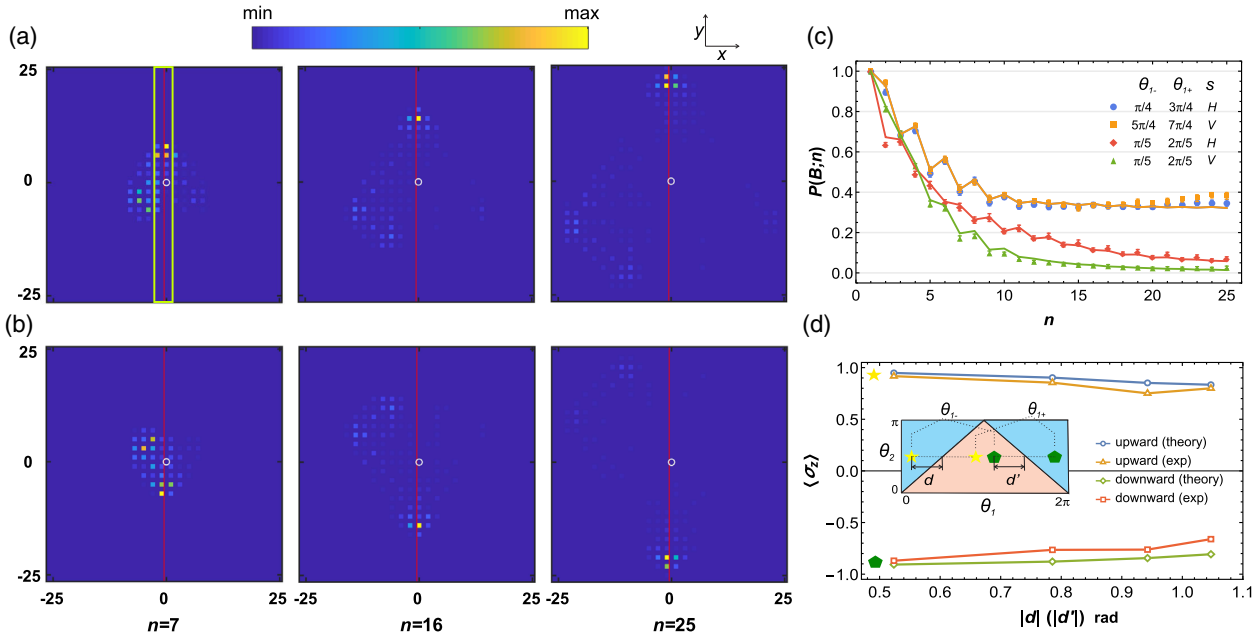

FIG. 3. Observation of spin-polarized chiral edge states in inhomogeneous 2DQWs. (a)–(b) Experimentally detected normalized probability distribution $P(x, y; n)$ after n steps with photons initialized at the origin (white circle), and parameters and initial polarization of: (a) $\theta_{1-} = \pi/4, \theta_{1+} = 3\pi/4, |H\rangle$; (b), $\theta_{1-} = 5\pi/4, \theta_{1+} = 7\pi/4, |V\rangle$. The red line at $x = 0$ indicates the boundary of inhomogeneous 2DQWs. (c) Evolution of the remained probability $P(B; n)$ within the boundary region as step numbers n increase. To calculate $P(B; n)$, probabilities in the boundary region B with a width of four lattice units [green unfilled rectangle in (a)] are summed. Quantum walks in (a) (blue circle) and (b) (orange square), as well as an inhomogeneous 2DQW without a topological edge (red diamond and green triangle), are shown. The parameters $\theta_{1\pm}$ and initial polarizations s (pseudospin) are annotated in the legend. Theoretical (experimental) values are depicted as solid lines (dots). (d) Plots of the average polarization in σ_z basis of photons remaining in edge-state wave packet after 25 steps as a function of the distance $|d|(|d'|)$ of $\theta_{1\pm}$ away from $\pi/2(3\pi/2)$. The values of $\theta_{1\pm}$ are symmetrically assigned around $\theta_1 = \pi/2(3\pi/2)$. The parameters we choose to obtain upward edge modes (yellow star), in turn, are $\theta_{1-} = \pi/3$ and $\theta_{1+} = 2\pi/3$, $\theta_{1-} = \pi/4$ and $\theta_{1+} = 3\pi/4$, $\theta_{1-} = \pi/5$ and $\theta_{1+} = 4\pi/5$, and $\theta_{1-} = \pi/6$ and $\theta_{1+} = 5\pi/6$. In terms of downward edge modes, all pairs of $\theta_{1\pm}$ are right shifted by π shown as the green polygons in the inset phase diagram. Statistical errors are smaller than the dot sizes.

measured probability distributions (P_{exp}) with the theoretically simulated distributions (P_{th}), we use fidelity $F(n) = \sum_{x,y} \sqrt{P_{\mathrm{th}}(x,y;n) P_{\mathrm{exp}}(x,y;n)}$. The fidelity of the spatial probability distribution of $P(x,y;25)$ (across 676 sites) in Fig. 3(a) [3(b)] is 0.960 ± 0.003 (0.950 ± 0.002).

In Fig. 3(c), we plot $P(B;n)$, the probability of finding the walker in the boundary region B [Fig. 3(a)] as a function of step number n. Half the width of B is set to 2 lattice units, which is larger than 1.3 lattice units, the typical decay length of edge states with quasienergies deep in the gap [31]. $P(B;n)$ for inhomogeneous 2DQWs in Figs. 3(a) and 3(b) tend to a constant around 0.35 after 11 steps [Fig. 3(c)].

On the contrary, when $H(\theta_{1-}, \theta_2)$ and $H(\theta_{1+}, \theta_2)$ are characterized by parameters from the same diamond of $W = -1$, the probability distribution spreads ballistically [31], which is a known feature of quantum walks [34]. The probability distributed in the vicinity of the boundary exhibits an approximately exponential decay for both initial states $|0,0,H\rangle$ and $|0,0,V\rangle$ [Fig. 3(c)]. As $|H\rangle$ and $|V\rangle$ form a complete basis for the internal degree of freedom, we conclude that, in this case, no edge modes exist near $x = 0$.

Notably, chiral edge states are spin polarized. In Fig. 3(d), we show that, as θ_{1-} and θ_{1+} are close to $\pi/2$ ($3\pi/2$), the internal states of edge modes are almost eigenstates of σ_z with eigenvalue $+1$ (-1). Moreover, polarization is associated with the chirality of the edge states; i.e., the spin component of edge states propagating in the $+y$ ($-y$) direction is almost $|\uparrow\rangle$ ($|\downarrow\rangle$), which is a result of the spin-orbit interaction inherent in the spin-dependent translation operations as Eq. (2). Depending on parameter choices, edge-state polarization can deviate from the eigenstates of σ_z [31,35].

Robustness of chiral edge states is revealed (Fig. 4) through changing the shape of the boundary by altering the voltage signal pattern applied to the EOM. As shown in

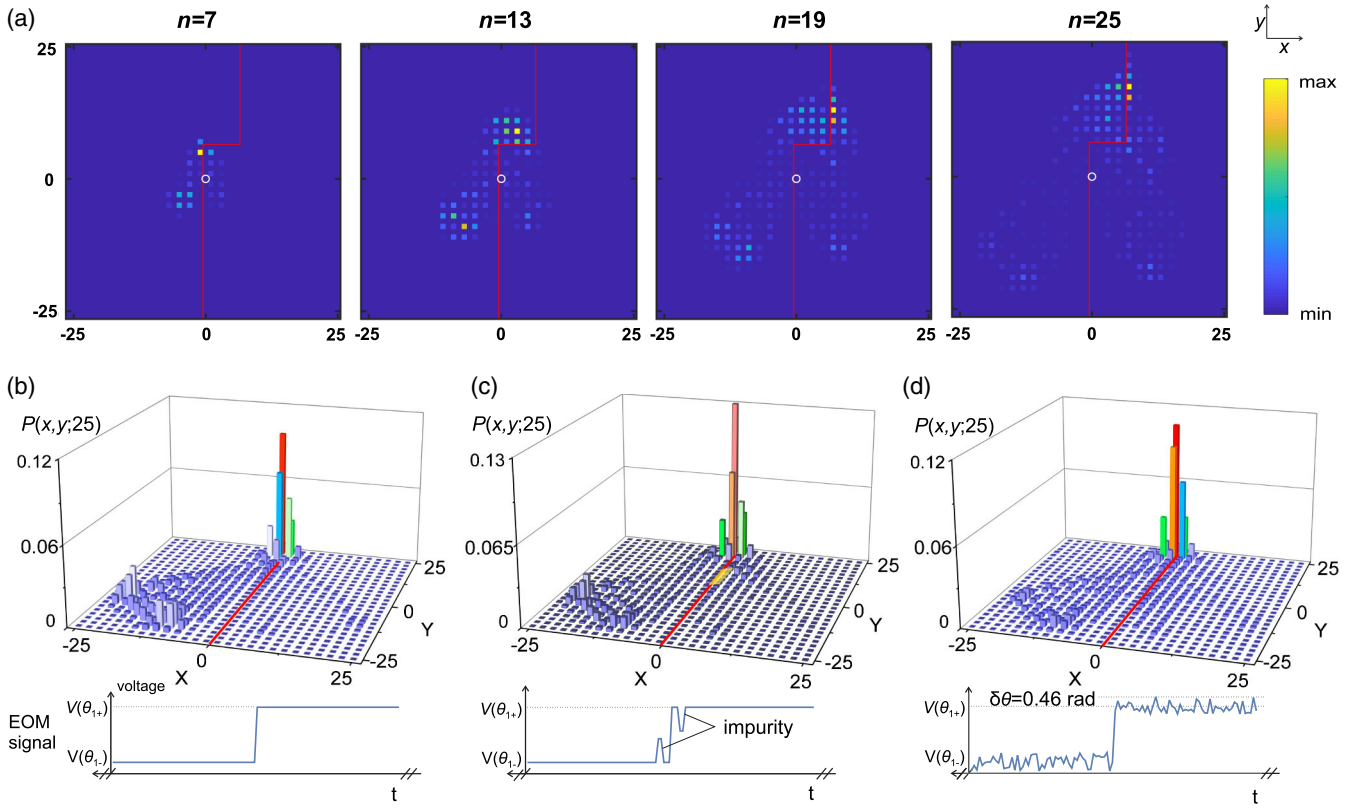

FIG. 4. Robustness of topologically protected edge states. (a) The measured probability distributions $P(x,y;n)$ of the inhomogeneous 2DQW with a boundary including two right angles, where the first right angle is at the position (0,7) and the second is at (7,7). The red line is to guide the eye. θ_1 for the left and right sides of the boundary are $\pi/6$ and $5\pi/6$, respectively. (b)–(d) The simulated [(b)] and experimentally measured [(c)–(d)] probability distributions $P(x,y;25)$ of the inhomogeneous 2DQW ($\theta_{1-} = \pi/4$, $\theta_{1+} = 3\pi/4$) with a straight-line edge at $x = 0$. Only odd sites are shown as the probabilities for even sites are zero. The schematic electro-optic modulator (EOM) signals of one step period are shown below the probability distributions correspondingly. In the theoretical simulation [(b)], a sharp boundary without impurities at the boundary and no disorder in the bulk are assumed. In (c), a 2×5-sized impurity is introduced along the boundary (marked as a yellow nub), where the on-site θ_1 is $\pi/2$. In (d), a noisy EOM signal is applied, corresponding to a spatially disordered rotation operation $R(\theta_1)$ where the value of θ_1 for each position (x,y) of $x < 0$ and $x \geq 0$ is randomly generated from the range of $(\theta_{1-} - \delta\theta, \theta_{1-} + \delta\theta)$ and $(\theta_{1+} - \delta\theta, \theta_{1+} + \delta\theta)$, respectively, where $\delta\theta = 0.46$ rad.

Fig. 4(a), the wave packet of edge states propagates along the irregular boundary with two right angles. The small mismatch between the experimental evolution path and theoretical prediction could result from the limited modulation speed of the EOM [31]. The fidelity of $P(x, y; 25)$ is 0.807 ± 0.002.

Furthermore, an impurity is introduced at the edge with on-site parameters dramatically different from those of both the left and right bulks, where the schematic EOM signal of one driving period is shown in the bottom half of Fig. 4(c). Scattering-free edge states are observed [Fig. 4(c)]. The fidelity of $P(x, y; 25)$ is 0.956 ± 0.002 compared to the theoretically simulated case without impurities [Figs. 4(b)]. Finally, we add random noise into the EOM signal [Fig. 4(d)]. To simulate the impact of spatial disorder, the noisy signal of a single step is repeatedly applied for 25 driving periods. A considerable probability of the walker remaining at positions near the boundary is detected and the final distribution has a fidelity of 0.931 ± 0.002 with that of Fig. 4(b). The insensitivity to dynamic disorder is also confirmed, where the spatial disorder is changing over time [31].

In conclusion, we implement inhomogeneous 2DQWs up to 25 steps with a time-bin encoded photonic circuit. Spin-polarized chiral edge states are observed at the interface between two topologically distinct quantum walk regions, and their robustness against various local perturbations is confirmed. Our results agree with theoretical predictions and demonstrate topological protection arising from the Rudner winding number rather than from the Chern number, which suggests that time-dependent dynamics during one driving period is crucial to understanding the topological classification of driven systems. Deeper understanding of the dynamical topological order and its extension to driven many-body systems require further theoretical and experimental investigation [36,37].

Our flexible scheme provides a proper platform for a systematic investigation of the topological phase transition of high-dimensional quantum systems [18,38–40], and for wide-ranging other quantum simulations [41–43]. We notice that similar experimental results are reported in Ref. [44].

We thank Bao-Zong Wang and Lin Wang for enlightening discussions. We also thank Wei-Wei Zhang for helpful discussion and comments on the draft. This work was supported by the National Natural Science Foundation of China, the Chinese Academy of Sciences, and the National Fundamental Research Program. B. C. S. acknowledges financial support from China's 1000 Talent Plan.

*dwwang@zju.edu.cn
†cylu@ustc.edu.cn
‡pan@ustc.edu.cn

[1] D. Pesin and A. H. MacDonald, Nat. Mater. **11**, 409 (2012).
[2] M. Z. Hasan and C. L. Kane, Rev. Mod. Phys. **82**, 3045 (2010).
[3] N. H. Lindner, G. Refael, and V. Galitski, Nat. Phys. **7**, 490 (2011).
[4] M. C. Rechtsman, J. M. Zeuner, Y. Plotnik, Y. Lumer, D. Podolsky, F. Dreisow, S. Nolte, M. Segev, and A. Szameit, Nature (London) **496**, 196 (2013).
[5] T. Kitagawa, E. Berg, M. Rudner, and E. Demler, Phys. Rev. B **82**, 235114 (2010).
[6] M. S. Rudner, N. H. Lindner, E. Berg, and M. Levin, Phys. Rev. X **3**, 031005 (2013).
[7] P. Titum, E. Berg, M. S. Rudner, G. Refael, and N. H. Lindner, Phys. Rev. X **6**, 021013 (2016).
[8] S. Mukherjee, A. Spracklen, M. Valiente, E. Andersson, P. Öhberg, N. Goldman, and R. R. Thomsonet, Nat. Commun. **8**, 13918 (2017).
[9] L. J. Maczewsky, J. M. Zeuner, S. Nolte, and A. Szameit, Nat. Commun. **8**, 13756 (2017).
[10] F. Wilczek, Phys. Rev. Lett. **109**, 160401 (2012).
[11] J. Zhang *et al.* Nature (London) **543**, 217 (2017).
[12] S. Choi *et al.* Nature (London) **543**, 221 (2017).
[13] F. Zähringer, G. Kirchmair, R. Gerritsma, E. Solano, R. Blatt, and C. F. Roos, Phys. Rev. Lett. **104**, 100503 (2010).
[14] A. Schreiber, K. N. Cassemiro, V. Potoček, A. Gábris, P. J. Mosley, E. Andersson, I. Jex, and Ch. Silberhorn, Phys. Rev. Lett. **104**, 050502 (2010).
[15] A. Schreiber, K. N. Cassemiro, V. Potoček, A. Gábris, I. Jex, and Ch. Silberhorn, Phys. Rev. Lett. **106**, 180403 (2011).
[16] A. Schreiber, A. Gábris, P. P. Rohde, K. Laiho, M. štefaňák, V. Potoček, C. Hamilton, I. Jex, and C. Silberhorn, Science **336**, 55 (2012).
[17] A. Crespi, R. Osellame, R. Ramponi, V. Giovannetti, R. Fazio, L. Sansoni, F. De Nicola, F. Sciarrino, and P. Mataloni, Nat. Photonics **7**, 322 (2013).
[18] T. Kitagawa, M. S. Rudner, E. Berg, and E. Demler, Phys. Rev. A **82**, 033429 (2010).
[19] T. Kitagawa, M. A. Broome, A. Fedrizzi, M. S. Rudner, E. Berg, I. Kassal, A. Aspuru-Guzik, E. Demler, and A. G. White, Nat. Commun. **3**, 882 (2012).
[20] F. Cardano, M. Maffei, F. Massa, B. Piccirillo, C. de Lisio, G. De Filippis, V. Cataudella, E. Santamato, and L. Marrucci, Nat. Commun. **7**, 11439 (2016).
[21] S. Barkhofen, T. Nitsche, F. Elster, L. Lorz, A. Gábris, I. Jex, and Ch. Silberhorn, Phys. Rev. A **96**, 033846 (2017).
[22] F. Cardano *et al.* Nat. Commun. **8**, 15516 (2017).
[23] L. Xiao *et al.*, Nat. Phys. **13**, 1117 (2017).
[24] E. Flurin, V. V. Ramasesh, S. Hacohen-Gourgy, L. S. Martin, N. Y. Yao, and I. Siddiqi, Phys. Rev. X **7**, 031023 (2017).
[25] K. v. Klitzing, G. Dorda, and M. Pepper, Phys. Rev. Lett. **45**, 494 (1980).
[26] D. J. Thouless, M. Kohmoto, M. P. Nightingale, and M. den Nijs, Phys. Rev. Lett. **49**, 405 (1982).
[27] T. Kitagawa, Quantum Inf. Process. **11**, 1107 (2012).
[28] J. K. Asbóth and J. M. Edge, Phys. Rev. A **91**, 022324 (2015).
[29] T. Groh, S. Brakhane, W. Alt, D. Meschede, J. K. Asbóth, and A. Alberti, Phys. Rev. A **94**, 013620 (2016).
[30] A. P. Schnyder, S. Ryu, A. Furusaki, and A. W. W. Ludwig, Phys. Rev. B **78**, 195125 (2008).
[31] See Supplemental Material at http://link.aps.org/supplemental/10.1103/PhysRevLett.121.100502 for more information about quasienergy band structures, quasienergy winding, analysis of the internal states of edge states,

experimental details, and extended data figures, which includes Refs. [5,32].
[32] J. K. Asbóth, L. Oroszlány, and A. Pályi, *A Short Course on Topological Insulators* (Springer International Publishing, New York, 2016).
[33] S. K. Goyal, F. S. Roux, A. Forbes, and T. Konrad, Phys. Rev. Lett. **110**, 263602 (2013).
[34] J. Kempe, Contemp. Phys. **44**, 307 (2003).
[35] J. Wu, J. Liu, and X. J. Liu, Phys. Rev. Lett. **113**, 136403 (2014).
[36] F. Harper and R. Roy, Phys. Rev. Lett. **118**, 115301 (2017).
[37] R. Roy and F. Harper, Phys. Rev. B **95**, 195128 (2017).
[38] A. Gómez-León and G. Platero, Phys. Rev. Lett. **110**, 200403 (2013).
[39] L. Michael, S. Christian, M. P. Hannah, Z. Oded, and B. Immanuel, Nature (London) **553**, 55 (2018).
[40] O. Zilberberg, S. Huang, J. Guglielmon, M. Wang, K. P. Chen, Y. E. Kraus, and M. C. Rechtsman, Nature (London) **553**, 59 (2018).
[41] J. M. Edge and J. K. Asbóth, Phys. Rev. B **91**, 104202 (2015).
[42] M. Di Liberto, A. Recati, I. Carusotto, and C. Menotti, Phys. Rev. A **94**, 062704 (2016).
[43] S. Takeda and A. Furusawa, Phys. Rev. Lett. **119**, 120504 (2017).
[44] B. Wang, T. Chen, and X. Zhang, preceding Letter, Phys. Rev. Lett. **121**, 100501 (2018).